





Article

Highly Efficient and Effective Process Design for High-Pressure CO₂ Photoreduction over Supported Catalysts

Matteo Tommasi ¹, Francesco Conte ¹, Mohammad Imteyaz Alam ², Gianguido Ramis ^{3,4,*}
and Ilenia Rossetti ^{1,2}

¹ Chemical Plants and Industrial Chemistry Group, Department of Chemistry, Università degli Studi di Milano, Via C. Golgi 19, 20133 Milan, Italy; ilenia.rossetti@unimi.it

² INSTM Unit Milano-Università, Via C. Golgi 19, 20133 Milan, Italy

³ DICCA, Università degli Studi di Genova, Via all'Opera Pia 15A, 16145 Genoa, Italy

⁴ INSTM Unit Genova, Via all'Opera Pia 15A, 16145 Genoa, Italy

* Correspondence: gianguidoramis@unige.it

Abstract: The photocatalytic reduction of CO₂ into solar fuel is considered a promising approach to solving the energy crisis and mitigating the environmental pollution caused by anthropogenic CO₂ emission. Some powder photocatalysts have been demonstrated as efficient, but their drifting properties, along with difficult separation (catalyst and product), make continuous mode reaction very challenging, particularly in the liquid phase. In order to make this process commercially viable and economically more efficient, we have developed a simple and scalable method for immobilizing TiO₂ P25 over the surface of glass slides using an organic-based surfactant. Improved adhesion properties and the homogeneous dispersion of catalyst nanoparticles were achieved. A holder was designed with 3D printing technology in such a way that it can hold up to six slides that can be dipped simultaneously into the suspension or solution of desired materials for a uniform and homogeneous deposition. The resulting surfaces of the dip-coated materials (e.g., TiO₂ P25) were further modified by adding metallic nanoparticles and thoroughly characterized via XRD, DRS UV-Vis, SEM, and SEM-EDX. Photocatalytic tests have been performed for two major applications, viz., hydrogen production via the photoreforming of glucose and the photoreduction of CO₂ into different solar fuels. The latter tests were performed in a specially designed, high-pressure reactor with Ag/P25 supported catalysts, which exhibited about three times higher formic acid productivity (ca. 20 mol/kg_{cat} h) compared to the dispersed catalyst, with enhanced stability and recoverability. It is to note that catalysts deposited on the glass slides can easily be recovered and the materials did not show any weight loss. To the best of our knowledge, the obtained formic acid productivity is highest among the published literature.

Keywords: CO₂ photoreduction; photoreforming; formic acid; photosynthesis; photocatalytic H₂ production; dip coating; coating of TiO₂



check for updates

Citation: Tommasi, M.; Conte, F.; Alam, M.I.; Ramis, G.; Rossetti, I. Highly Efficient and Effective Process Design for High-Pressure CO₂ Photoreduction over Supported Catalysts. *Energies* **2023**, *16*, 4990. <https://doi.org/10.3390/en16134990>

Academic Editor: Jacek Grams

Received: 2 May 2023

Revised: 15 June 2023

Accepted: 16 June 2023

Published: 27 June 2023



Copyright: © 2023 by the authors. Licensee MDPI, Basel, Switzerland. This article is an open access article distributed under the terms and conditions of the Creative Commons Attribution (CC BY) license (<https://creativecommons.org/licenses/by/4.0/>).

1. Introduction

The global energy shortage and environmental pollution due to heavy reliance on limited fossil fuels are key challenges facing mankind. To fulfill ~82% of our total energy demand, 12 million tons of oil, 22 million tons of coal, and 10 m³ of natural gas are consumed every day [1,2]. Unfortunately, when energy is extracted from these resources, a large volume of CO₂ is emitted. This causes environmental concerns, including global warming, ocean acidification, and the related macroscopic effects they induce [3]. In the past century, and in particular during the last two decades, the Earth's surface temperature has steadily increased. This has been univocally correlated with increasing anthropogenic CO₂ emissions, which recently surpassed 400 ppm concentration in the atmosphere, which was considered a threshold of non-return. Finding an alternative energy resource with

advancements in technological development could pave the way toward solving this challenge with a sustainable supply of fuels and chemicals. The use of photovoltaic panels [4] to exploit solar energy is one of the options, but intermittency issues and the requirement of a large area are key concerns. As a result, research on photocatalysis as a way to store solar energy in chemical form has gained momentum [5] to exploit solar light storage in chemical form for use when sunlight is not available. Its major applications are the production of renewable hydrogen via the photoreforming of organic molecules and various oxygenated products produced through CO₂ photoreduction to solar fuel using semiconductor-based heterogeneous photocatalysts. Since this process utilizes CO₂ as feedstock and turns it into advanced fuel or renewable chemical reagents, such as formic acid, formaldehyde, and methanol (Scheme S1, Supplementary Information File), under mild conditions (<100 °C) using water as a solvent [5–9], improved environmental sustainability is expected [3].

Water photosplitting is another very interesting process for obtaining solar fuels (i.e., H₂), though very low hydrogen productivity has been reported. This is due to the faster recombination of electrons and holes after their production via the photoexcitation of a semiconductor photocatalyst. The charge's relaxation is typically faster than the reactions to be promoted [10–14]. Different organic compounds have been proposed as hole scavengers to improve the rate of reaction, and carbohydrates represent an interesting option that allow for the exploitation of waste aqueous solutions (e.g., from the paper, milk, and food industries).

Most of the available literature dedicated to photosynthetic applications has relied on titania based materials in cases where it is added with metal co-catalysts or coupled in a Z-scheme with a small band gap semiconductor to improve visible light harvesting. Evonik P25 TiO₂ powder is often used for photocatalytic applications as it is a commercial, widely available, and reproducible material. P25 is prepared through the hydrolysis of an aerosol of a titania precursor (TiCl₄) [15]. It structurally comprises a mixture of anatase and rutile (ca. 3:1). The higher photocatalytic activity of P25 compared to pure anatase and rutile titania has been attributed to the passage of electrons from one phase to the other, thus improving charge separation and leading to the stabilization of photogenerated charges for a longer time than in pure phases [11,16,17].

As a drawback, the use of nanosized photocatalysts in the form of powder is fine for testing the intrinsic activity of the catalyst in batch small scale thanks to its high surface area and maximum exposure to the light, but it is not at all feasible for large scale and continuous processes. Indeed, it is very challenging to recover or recycle a photocatalyst after the end of the process, which in turn results in increased costs and longer processing times [18]. An immobilized photocatalyst is further required for all processes that involve the treatment of a gaseous phase, for instance, CO₂ photoreduction [19,20].

Several techniques can be exploited for the immobilization of the photo-active phase, from the well-established sol-gel synthesis and solvent deposition to the more sophisticated ones, such as chemical and physical vapor deposition (CVD, PVD) [19]. Other deposition methods involve the insertion or anchorage of the photocatalyst NPs to a polymeric membrane [18]. All these methods are quite sophisticated and poorly adaptable to large scale devices. Furthermore, though surface deposition techniques are widely studied in catalysis, photocatalytic reports over supported photocatalysts are not frequent and particularly scarce for the two mentioned photosynthetic reactions.

In this work, an attempt has been made to solve the complexities involved with catalyst immobilization while improving productivity and the recovery of desired products and photocatalyst recycle. The developed system can adapt well to future applications with gas phase testing or continuous operations. Our process of dip coating nanomaterials integrated with 3D-printed holders is simultaneously very simple and matches with a unique, high pressure photoreactor technology. It is here validated as a straightforward and scalable way to produce solar fuels (hydrogen, formic acid, formaldehyde, and methanol) via the photoreforming of glucose and the photoreduction of CO₂.

2. Materials and Methods

2.1. Materials Used

Commercial TiO₂ P25, produced by Evonik (formerly Degussa, Essen, Germany), and supplied by Eigenmann and Veronelli S.p.A. (Istanbul, Turkey), was used as a benchmark.

Hydrogen (H₂), helium (He), and carbon dioxide (CO₂), all with a purity >99%, were purchased from AirLiquide (Milano, Italy).

Microscopy glass tiles (size 26 × 76 × 1 mm), purchased from Pearl[®], were used as supports for catalyst immobilization. H₂SO₄ (Sigma–Aldrich, Merck KGaA, Darmstadt, Germany, 98%) and H₂O₂ (Sigma–Aldrich, Merck KGaA, Darmstadt, Germany, 30%) were used to clean the glass tiles before deposition.

Disperbik[®] was used as an emulsion stabilizer to increase the loading of titania during deposition. HCl (Sigma–Aldrich, Merck KGaA, Darmstadt, Germany, 37%) or NaOH (Sigma–Aldrich, Merck KGaA, Darmstadt, Germany, 98%) were used to tune the pH of the titania suspension. AgNO₃ (Sigma–Aldrich, Merck KGaA, Darmstadt, Germany, 99%) was used to perform the metal deposition.

A carbolite tubular oven was used to perform a reduction of the deposited metal oxides.

The supports for dip coating and for the glass tiles were 3D printed in either PLA or polypropylene reinforced with glass fibers. The final model in stainless steel was realized using “EuroGalvano S.r.l.,” sited in Lodrino, Italy. The 3D printing was performed with the 3D printer model “Metal X”.

2.2. Catalysts Characterization

X-ray diffraction (XRD) analyses were performed with a Miniflex-600 horizontal-scan powder diffractometer (Rigaku, Tokyo, Japan) using Cu-K α radiation with a graphite monochromator on the diffracted beam. The crystallite size was calculated according to the Scherrer equation, Equation (1).

$$D = (K \lambda) / (\beta \cos \theta) \quad (1)$$

where D is the crystal size, λ is the X-ray wavelength (0.154 nm with Cu K α generator), K is the shape factor (0.9), β is the width at half maximum of the peak (i.e., FWHM), and θ is the Bragg angle.

Diffuse reflectance (DR) UV–Vis spectra of samples were recorded on a UV-3600 Plus (Shimadzu, Kyoto, Japan) in the range of 200–800 nm, using an integrating sphere and BaSO₄ as the reference standard. The results were processed according to the Kubelka–Munk elaboration and with Equation (2), using the reflectance spectra as input data [21].

$$F(R_{\infty}) = (1 - R_{\infty})^2 / 2R_{\infty} \quad (2)$$

The calculated $(F(R)h\nu)^{1/r}$ (with $r = 2$ or $\frac{1}{2}$ for direct and indirect band gaps, respectively) was plotted versus $h\nu$ to obtain the band gap of each sample according to the Tauc Equation (3) [22].

$$(F(R)h\nu)^{\frac{1}{n}} = B(h\nu - E_g) \quad (3)$$

All the samples were diluted one-to-one or one-to-two with BaSO₄, the reflectance standard that prevents saturation when mixed with samples that absorb too much. Therefore, the shape of the curves was not affected by the blending, but the absolute value of reflectance cannot be compared.

Scanning electron microscopy (SEM) images and energy dispersive X-ray analysis (EDX) spectra were obtained using a JSM-7900F Schottky field emission scanning electron microscope (JEOL, Tokyo, Japan) operating at an accelerating potential of 20 kV.

2.3. Photocatalytic Activity Testing

All the experiments were performed in a specially designed photoreactor developed by our group [23] that allows for operation under high pressures, up to 20 bar, and temperatures up to 100 °C. The reactor is equipped with a thermostatic bath, through which water circulates to the reaction vessel via the envelope/jacket and maintains the desired temperature. The photoreactor is a cylindrical shaped vessel made of AISI 316 stainless steel. The gross internal volume of the reactor is equal to 1.7 L, and the net volume is equal to 1.3 L as a result of the presence of a quartz candle immersed in the liquid. The latter, which contains a two-bulb, 125 W, medium Hg-pressure UV lamp, allows for the protection of the lamp from high pressures and the axial irradiation of the reaction mixture simultaneously. The radiation is emitted in the range of 254–365 nm. The irradiance of the lamp was checked periodically using a photoradiometer (Delta OHM HD2102.2, equipped with an LP 471A-UVeff probe, RS Components S.r.l., Sesto San Giovanni, Italy), sensitive in the range of 250–400 nm, resulting in average of 120 W/m². The reaction mixture was continuously stirred at 400 rpm in order to ensure a homogeneous dispersion of the solid catalyst in the liquid phase.

In the upper part of the reactor, a gas inlet was placed to bubble the gas through the solution during the loading cycle when operating in batch mode, or to continuously feed the reactants in continuous mode. The gas outlet was placed on top of the reactor and was connected to a sampling section equipped with a manometer that allowed for the measurement of pressure inside the reactor.

2.3.1. Photoreduction of CO₂

In a typical procedure, 1.2 L of an aqueous Na₂SO₃ (1.66 g/L) solution (as optimized previously [16,24–26]) and the desired quantity of the photocatalyst, i.e., 0.031 g/L in the case of a powder catalyst, were charged into the reactor. Na₂SO₃ was used as a hole scavenger. Moreover, a magnetic bar was placed inside the vessel, and the system was able to heat under the desired conditions (temperature, time, and pH) with 8–18 bar of CO₂ pressure. Photocatalytic tests were performed either at neutral or basic pH (pH = 14). Under basic pH, NaOH was used to maintain the required pH values [16,24–26]. Each experiment was carried out for 6 or 24 h. After testing, the lamp was shut off and the reactor cooled to an ambient temperature before we proceeded with the samplings. Gaseous products were analyzed with a GC Agilent 7890A equipped with two columns (HP PlotQ and MS, both 30 m long), two detectors (FID and TCD), and a sampling loop of 250 µL (SRA Instruments, Cernusco sul Naviglio, Italy). The liquid samples were centrifugated at 10,000 rpm for 15 min to remove the nanosized photocatalyst present in the suspension. An iodometric titration was performed to quantify the sodium sulfite conversion. The samples were also analyzed via HPLC with a Jasco instrument (Sintak Srl, Corsico, Italy), including an injection sampling loop of 20 µL, a precision pump (PU-4180), and a polymeric column (SepaChrom Benson Polymeric BP-OA BL0053 2000-0, Sintak Srl, Corsico, Italy) with a stationary phase of PS-DVB sulfonated gel (dimension 300 × 7.8 mm) immersed in a thermosetting bath kept at 45.6 °C. The liquid was analyzed using a UV-Vis detector and a refractive index (RI) detector (Sintak Srl, Corsico, Italy). The wavelength of the UV-Vis detector was fixed at 210 nm in order to analyze the amount of formic acid obtained from the analysis with more accuracy.

2.3.2. Photoreforming of Glucose

Glucose (anhydrous, pur. 96%) was supplied by Sigma-Aldrich and diluted at 5 g/L with deionized water. The reaction mixture was stirred by means of a magnetic stirrer placed inside the reactor, and N₂ was used for degassing and pressurizing at 5 bar. A temperature of 80 °C, the desired amount of the photocatalyst (0.25 g/L when operating with catalyst powder), and its naturally established pH were the optimized operating conditions. Tests lasted for 5 h of irradiation, if not otherwise specified [10,11].

The gas and liquid phases were analyzed via GC and HPLC on the same instruments described in the previous section. HPLC was calibrated for the quantification of glucose, arabinose, and cellobiose. As a result of the wide spectrum of possible oxidation intermediates, the carbon conversion was also determined by analyzing its total organic carbon (TOC) and, therefore, its conversion.

A total of 5 mL of solution taken at 0 and 5 h were placed in glass vacutainers. Then, 5 mL of 0.178 M $K_2Cr_2O_7$ solution and 5.5 mL of concentrated H_2SO_4 (96%) were added. In a third vacutainer, only $K_2Cr_2O_7$ solution and sulfuric acid were added as blanks. All vacutainers were placed in a digestion oil bath and heated at 130 °C for 30 min. The resulting solutions were analyzed in a Lambda 35 double ray UV–Vis spectrophotometer at 605 nm (Perkin Elmer Italia, Milan, Italy).

A Shimadzu TOC-L CSH/CPH was also used to test 50 mL aliquots of a 1:20 diluted sample prepared from the solution spilled from the reactor.

3. Results

3.1. Design of Reactor Supports

Because of the cylindrical shape of the jacketed, stainless steel, pilot photoreactor, a circular sample holder was designed in order to employ deposited glasses for carbohydrate photoreforming and the CO_2 photoreduction reactions. The sample holders were specially designed with a 3D-modeling software (SketchUp) in order to fit around the quartz sleeve that contains the lamp. First, the internal volume of the photoreactor was simulated, and it was found that the maximum number of glass slides that fit the internal volume without touching the lamp, the reactor cap, or the magnetic stir bar was 24, distributed on four levels. For this reason, a first design of the support was elaborated, later simplified based on the maximization of free volume and exposition to light bulbs [27].

For this reason, the design shifted towards the use of two separate layers, each one able to hold six glass tiles. After many optimization steps, a final design was obtained, reported in Figure 1. This final version consisted of two separate layers, each one in the shape of an open ring, equipped with a small clip that allowed it to directly attach to the support for better stability (Figure 2a).

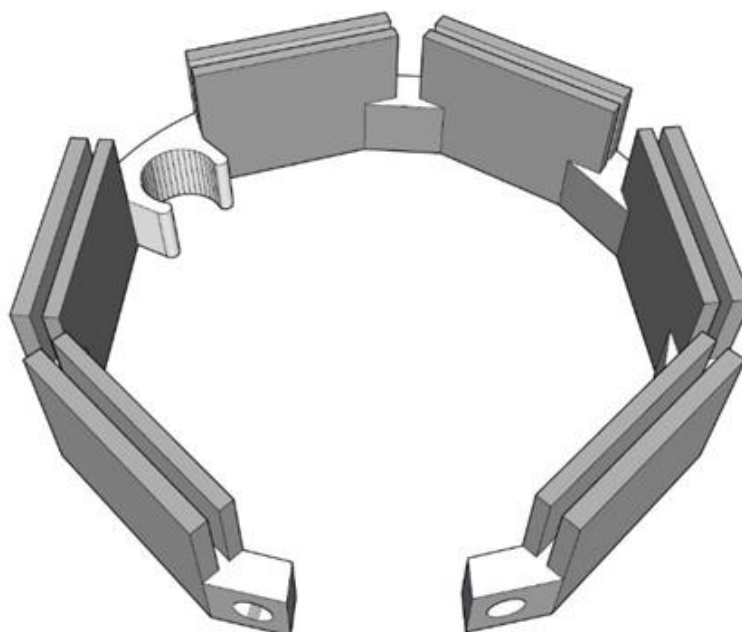


Figure 1. Final optimized design of the glass tile holder.

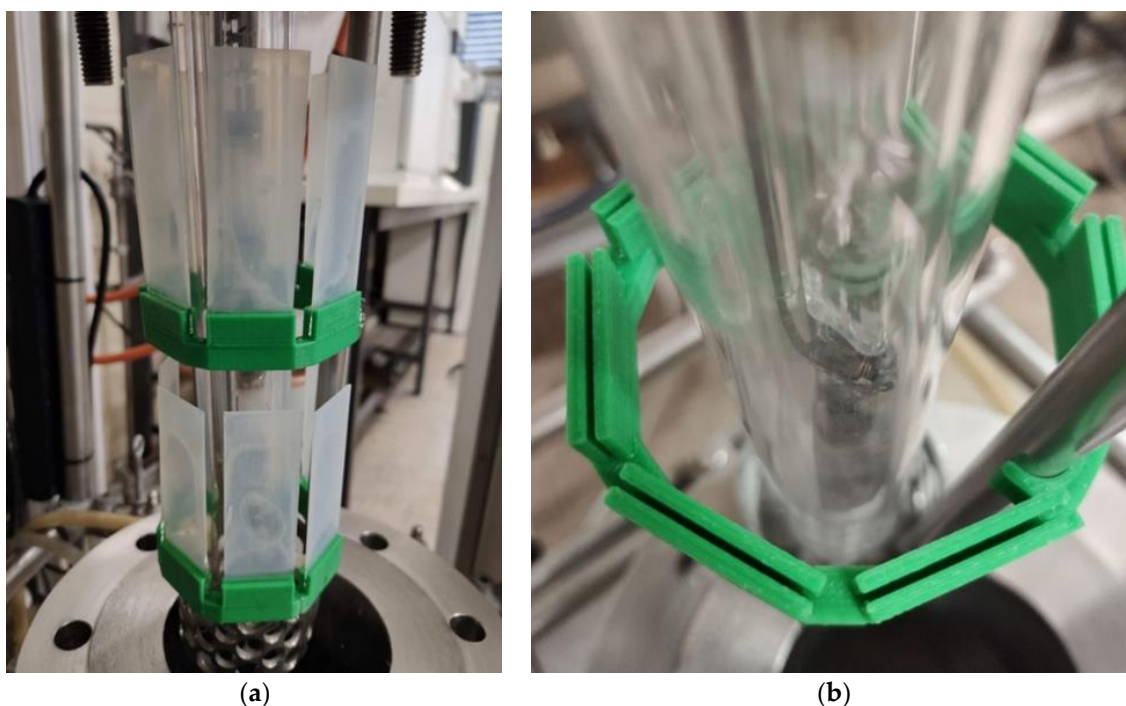


Figure 2. (a) Final version of the support printed and set up in ABS; (b) Detail of the clip connection to the shaft.

In order to test the proposed design, we took advantage of a 3D printing technique, which is inexpensive and fast, considering the small size of the tools that we needed. In particular, after printing test models with PET and ABS, two different 3D printing materials were used. The first model was realized in polypropylene (PP) mixed with glass fiber. The latter support was tested multiple times in the photoreactor and it proved stable under the reaction conditions employed for the photoreduction of CO₂ (80 °C). A second model was then 3D printed in stainless steel for more general applications at even higher temperatures. The stainless steel used for the 3D printing was the 17-4 PH one, which is a low carbon steel with the following composition: 15–17.5% Cr, 3–5% Ni, 3–5% Cu, <1% Si, <1% Mn, 0.15–0.45% Nb, 0.07% C, and traces of phosphorous, sulfur, and iron to reach 100%.

An example of the complete setup is reported in Figure 2a. The glasses were inserted through the uncoated area and placed right in front of the bulb. In addition, Figure 2b illustrates the connection on the shaft through the clip on the ring.

3.2. Set Up and Optimization of the Catalyst Deposition Process

The supports employed in this work were glass slides typically used in microscopy with the dimensions of 26 × 76 × 1 mm³ because they are inexpensive and easily available in the market. The deposition was performed through a homemade dip coating apparatus, and a suspension of P25 powder in distilled water was used as a base for the impregnation of the glasses.

Different coating procedures have been reported in the literature for obtaining structured catalysts or microchannel reactors. They have been extensively reviewed in [28] for the most frequent applications. Surface pretreatment is often suggested to increase the roughness, which is achieved via a thermal pretreatment (e.g., oxidation at high temperatures), anodization (suitable only for metals, e.g., Al), and an acid treatment (used here, as it is the only one applicable to glass substrate). The suspension method allows for the covering of the substrate with a pre-synthesized catalyst, and it is, therefore, possible to learn and control the main features of this catalyst via basic characterization. On the contrary, a sol-gel technique can be adapted to form the catalyst (oxide) directly over the surface that will be coated; however, using this method, the properties of the material are

less easily predictable and controllable. Both these methods and some hybrid variants have been applied to the coating of TiO_2 . Electrophoretic and electrochemical plating have usually been applied for coating over-conducting substrates and for the deposition of metal layers. Impregnation can be used to support metals or oxide precursors over porous supports, but it does not fit glass supports unless a porous material has been previously added. For instance, it can be used for the addition of metal promoters over an oxide semiconductor coating. Chemical or physical vapor deposition (CVD or PVD) may be suitable solventless deposition techniques when volatile precursors are available. A more complex and dedicated apparatus is needed with respect to the previously described methods. Overall, the suspension technique allows researchers to obtain, in an easy and rapid way, relatively thick coatings (ten-hundreds of microns) of oxides over any kind of surface, making it a quite simple and scalable technique.

The homemade dip coating apparatus, equipped with a 3D-printed adapter, allows for the processing of up to six samples at the same time. A typical immobilization experiment consists of the immersion of glass tile(s) at a selected constant speed by means of a step motor equipped with reducing gears. The composition of the mother suspension was optimized during the study.

The first coatings were applied to the untreated tiles through several subsequent dipping cycles, as reported in Table S1 (Supporting Information File).

In the blank experiment, the glasses dipped into distilled water and dried at $500\text{ }^\circ\text{C}$ under air did not show any weight variation. On the other hand, after the first cycle of dipping with P25/water suspension at a $5\% w/w$, an average loading of 0.7 mg of powder per tile was obtained with a $\pm 0.1\text{ mg}$ discrepancy after tens of repetitions.

This P25 suspension was selected as it is fairly stable once the mechanical stirring is halted, allowing us to carry out the dipping while avoiding a massive precipitation of the titania, which could impact the reliability of the deposition itself. The tiles were clamped on the top, so the resulting powder was distributed over approximately 80% of the surface. Two cycles only led to a slight increase in the deposited P25, up to 1.2 mg , with a mean value of 0.9 mg ; thus, the deposition after each cycle was ca. 0.5 mg . It is noteworthy to point out that the deposited layer was not homogeneous. A closer analysis with an optical microscope (up to $\times 400$ magnification power) unveiled that the surface of the glasses was unfinished, and many microscopic debris prevented the homogeneous deposition of the P25 nanoparticles (Figure 3b).

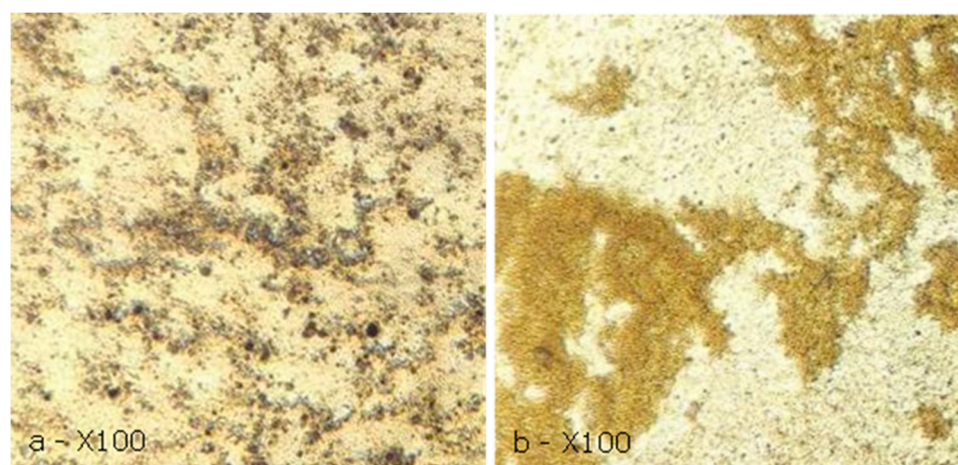


Figure 3. P25 photocatalyst deposited over glass surface after two cycles, (a) washed with piranha solution, and (b) untreated surface. Observed through an optic microscope at 100 magnification power.

To overcome this problem of non-homogeneity, all the glass slides were pretreated and washed with a piranha solution ($3:1\text{ H}_2\text{SO}_4/\text{H}_2\text{O}_2\text{ }30\% w/w$), which proved to be effective

in cleaning and activating the surface to adhere the catalyst. Interestingly, a significant improvement in the coating over the glass surface was observed with an average of 2.3 mg of P25 deposition in two consecutive cycles.

Interestingly, the first deposition did not deposit an appreciable amount of titania, barely 0.1 mg (Table S1, Supporting Information File), which is probably due to the left-over traces of piranha solution on the surface. After three deposition cycles, the average photocatalyst layer weight (2.2 mg) was lower than that of the same layer after two cycles, which was 4.8 mg, and we interpreted this as being a result of the fact that some titania was detached again during the subsequent dipping as a result of poor adhesion of the first layer. In any case, at the end of the 6th cycle, the average layers weighed 5.5 mg.

To confirm the hypothesis that traces of piranha solution were interfering with the deposition process, the tiles were rinsed with sodium carbonate solution (1 M) and then dipped into the P25/water suspension. This was selected as a weak and inexpensive base, able to tune the surface charges. After three cycles of coating, the average deposition was 3.4 mg, almost 50% higher than the amount that was previously obtained (2.2 mg).

The positive effect of rinsing can possibly be explained by the effect of acids or bases on the surface charges present on the glass surface [29]. The point of zero charge of borosilicate is ca. 7.5–8, while that of P25 Titania is ca 6.5 [30]. When treating the glass surface with piranha solution, besides removing impurities, we left the surface enriched with positive charges and enriched it with oxydrils after rinsing with carbonate. This may have affected the surface interaction with suspended particles that, depending on the pH of the slurry, may have been neutral or positively or negatively charged. Since the pH of the slurry was ca. 5.5 when native pH was kept in the deionized water, the P25 particles were positively charged and may have interacted more favorably with a surface where an excess of positive charges, attained after treatment with a strongly acidic solution, had been neutralized with carbonate.

One doubt may regard the chemical effects of residual amounts of piranha solution, particularly sulfur. This is in general not considered a problem, since the reaction of CO₂ photoreduction is carried out using a significant amount of sulfite as the hole scavenger, which oxidizes to sulfate. Therefore, it is very unlikely that possible residuals at the interface between the glass and the coated powder exerted a significantly different effect in such a surrounding. This notwithstanding, we checked the effects of glass cleaning with the piranha solution and subsequent washing by performing EDX analyses (Figure S1), reported in the Supporting Information File. A significant concentration of sulfur was noticed only for the sample immediately after treatment with the piranha solution. Subsequent rinsing and washing progressively decreased the S content down to 2 wt% (only one washing with water) or to negligible concentrations for further washing with bicarbonate and then with HCl (See Figure S1, Supporting Information File).

Other researchers reported a simple coating technique with a brush rather than a dip coating apparatus, so that route was explored as well [31]. This is an interesting procedure for coating only the catalyst where needed (e.g., over one side of the tile only). Unfortunately, despite a mean deposition weight of 6.3 mg after just one cycle, this technique was not reliable, since the layer of titania was less uniform even with respect to the untreated tiles processed via dip coating.

In light of these results, more tests were developed to assess the robustness of the double washing (piranha solution and rinsing with carbonate) procedure. As reported in Table S2 (see Supporting Information File), an average of 0.7 mg was added after each cycle, and this was consistent among the series of four glasses, even with a sparse standard deviation. The standard deviation was further optimized, increasing the amount of coating. Six cycles allowed for the collection of 4.2 mg of P25 deposited over the surface of the tiles, which is in line with our requirements as the photocatalytic reduction of CO₂ was previously optimized using 37 mg of photocatalyst powder in 1.2 L of solution. By using 12 tiles with such coatings, a consistent comparison could be ensured.

Not only did the deposited layer result in being very homogeneous, it was also sufficiently resistant from an adhesion point of view. This point was first demonstrated via the immersion of a glass tile in a beaker containing water and maintaining stirring for 3 h. After that amount of time, the glass tile was dried at 105 °C and weighed again, which confirmed that no appreciable amount of coating was lost during the tests (reproducibility was ensured by many repetitions), at least within the limits of the balance used, i.e., 0.1 mg precision. In addition, an abrasion resistance test was carried out. Scratch and abrasion tests are codified differently according to the purpose of the abrasion resistance measurement. Evaluations of the resistance to abrasion and the hardness of the coating are the most important features in this case, which are measured by applying a constant force and measuring the loss of powder, since the coating should not be purposefully used in contact with other surfaces. On the contrary, for surfaces that should be used in continuous contact with other solid objects, an increasing force is applied until the coating is lost completely or up to a predetermined % of weight.

In our measurement, the coating was subjected to a constant small force, and the loss of powder was measured. For this, we used a homemade apparatus comprising a 500 mm-long plane inclined at 45° and covered with sandpaper (P200). With this setup, each tile was pulled down the plane by its own weight (ca. 5 g mass, ca. 0.06 N scratch force on the inclined plane), and as a result, roughly the same force was applied during the tests. Then, the tiles were weighed and observed with a microscope. The surface of the glass tiles was unaffected based on the observation with a microscope.

Even after multiple abrasion cycles, none of the glasses lost more than 0.1 mg of coating, and the surface was substantially unaffected. Given the robustness of the deposition technique, we decided to further optimize the parameters to obtain a higher loading of TiO₂ per cycle.

All the following tests were performed using two deposition cycles. Table S3 (see Supporting Information File) summarizes all the results, which show that there is an effect of the solution temperature on the deposition of P25. For instance, the weight of the deposited layer increased by 20% when the temperature rose to 30 °C and by 87% with a further increase to 50 °C. Both the minimum and the maximum weights of the series (usually composed of twelve samples) increased as well.

Another important parameter was pH, which was lowered via the addition of either HCl or HNO₃, which are both strong acids and widely used for activating glass, with the former being, in general, more volatile [32]. It was found that a lower pH was favorable for the deposition process, with a mean weight of 3.6 mg (+29% vs. 50 °C @pH7) for HCl and 4.0 mg (+43% vs. 50 °C @pH7) for HNO₃. However, this second set of samples showed a rough surface and lumpy areas, and a moderate increase in weight with respect to the samples treated with HCl and a significant loss of homogeneity of the surface was observed.

Conversely, the deposition carried out at pH 12 via the addition of ammonia led to a modest increase in the deposited layer, equal to +11% or 3.1 mg in total. This is in line with the already discussed effect of pH on the surface charge density of particles. At pH > 8, the surfaces of both glass and titania particles are negatively charged, disfavoring a surface interaction, at least of electrostatic nature [29,33,34]. In addition, the surface was even less homogeneous; thus, the best option was represented by the addition of HCl and the dip coating performed at 50 °C. As expected, many subsequent cycles of deposition led to a remarkable increase in the overall weight of the titania layer, up to 10.7 mg after six treatments (Table S4, see Supporting Information File).

So far, 5% *w/w* has represented the maximum TiO₂ concentration to avoid the massive precipitation of titania in the absence of stirring. To try to overcome this limit, thus improving the amount of titania loading per cycle, we tested an industrial emulsifying agent for paints based on titanium dioxide named Disperbyk-190[®]. This is an organic-based compound that stabilizes the water suspension of titanium dioxide when added up to 3%

w/w_{TiO_2} . By using Disperbyk-190[®], it was possible to increase the concentration of the suspension up to 25% w/w without significant precipitation.

Different suspension concentrations were tested, and Table 1 summarizes the results achieved using P25 suspensions in the range of 5–25% w/w . At ambient temperatures and after two deposition cycles, the average weight of the deposited layer was almost 30% higher than our benchmark at 5% w/w , but still 1.5 times lower than the weight obtained using HCl at 50 °C. However, thanks to the additive, it was possible to match the performance of the latter setup simply by increasing the amount of titania added to the water to 10% w/w . In addition, when this ratio was set to 15.5% the average weight of the P25 deposited over the glasses increased three-fold (12.6 mg vs. 4.3 mg). Lastly, by pushing the system to the limit with a 25% solution of P25 in water, it was possible to obtain a very thick deposited layer, equal to 100 mg per tile, that, although very homogeneous, was quite fluffy and easy to peel off if accidentally touched. In light of these results, we concluded by performing just one impregnation with a suspension of 15% (w/w) to ensure proper adhesion to the glass surface.

Table 1. Photocatalyst loading over glasses obtained via dip coating in 5–25% w/w P25 and Disperbik-190[®] suspension in distilled water. Post-treatment was performed in a furnace at 500 °C for 1 h.

Recipe No.	% w/w	N ^o Cycle	Av. Loading (mg)	Min (mg)	Max (mg)
12	5.1	2	2	1.0	3.1
13	10.0	2	4.3	3.4	5.2
14	15.5	2	12.6	6	22.9
15	25.3	2	100.6	89.1	112.8
16	13.7	1	4.0	3.2	4.7

3.3. Supported Photocatalysts Functionalization

P25 photocatalysts have some limits in their applications as a result of their poor harvesting of solar light, limited to the UV fraction only, and fast electron–hole recombination. Metallization is often reported as a strategy for improving an electrons lifetime, since metals with the appropriate work function act as electron sinks, avoiding their recombination with the holes. Furthermore, metal nanoparticles that exploit plasmonic resonance may add additional “hot electrons” that are activated under visible light.

The bare P25 catalyst deposited over the glass tiles was then further functionalized by impregnation with Ag via immersion into a solution of precursor. According to the literature and to previous experiments by our group, it could be hypothesized that the photopromoted electron in the semiconductor would transfer to metal particles, avoiding direct relaxation, to recombine with the hole. The electron could then be used for the reduction half-reaction when the reactant is adsorbed over the metal cluster.

The first impregnation experiment was carried out by dip coating glass tiles in a 13.7% (recipe #16) solution of titania in water (with Disperbik-190[®] used as additive), followed by a second cycle of impregnation after treatment in the muffle at 500 °C with a 0.07 M water solution of silver nitrate. The slides were then dried for 1 h at 105 °C and placed in a tubular oven to perform the reduction under a hydrogen atmosphere (5 °C/min ramp, 150 °C, 30 mL/min H₂). At the end, some slides were carefully scratched in order to recover the catalyst, and the resulting powder was analyzed by means of XRD, DRS, and SEM-EDX techniques.

3.4. Materials Characterization

3.4.1. XRD Analysis

XRD analyses were performed on both the commercially available P25 and the same photocatalyst deposited over the glass tiles. In order to perform the analysis of

the deposited catalyst, the powder was scratched from the glass tiles with the help of a stainless-steel spatula.

The XRD were comparable, and the only thing that differed was the amount of anatase and rutile with the deposited P25, which increased the anatase phase after thermal calcination. Normally during calcination at high temperatures, the transformation of anatase to rutile is favored. Some authors have reported that, during calcination at high temperatures, transformation of the amorphous phase to anatase and anatase to rutile occurs [35,36]. The latter transformation has been reported in the temperature range of 600–1100 °C. Amorphous phase-to-anatase transformation is reported to occur in the range of 350–450 °C. This suggests that, because of the relatively low temperature of calcination, 500 °C, some amorphous phase could have been converted to anatase, leaving the rutile unaffected. Results are reported in Figure 4.

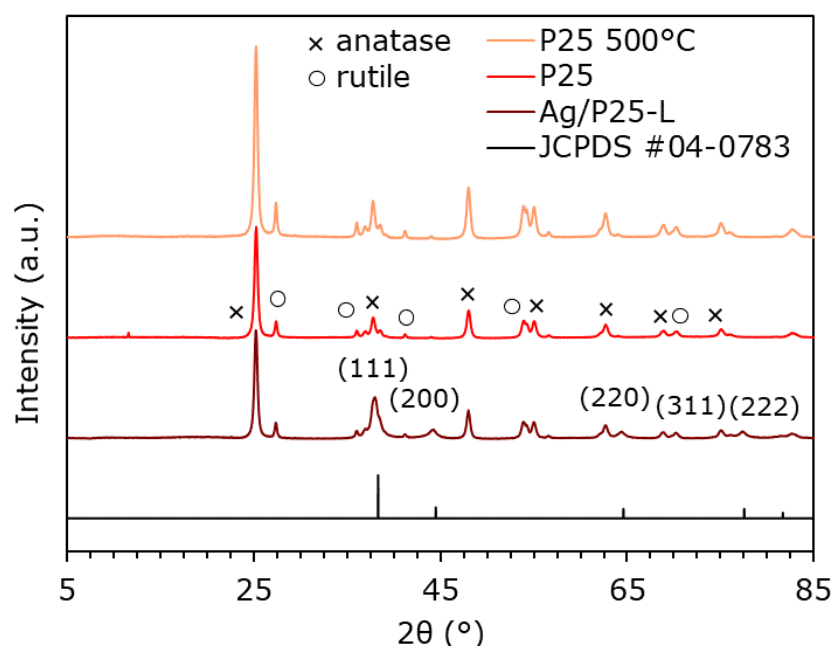


Figure 4. Diffraction patterns of P25 and Ag/P25 deposited over glass slides (JCPDS card #085-1326 for reference), compared with the commercial P25.

When loaded with Ag, a diffractogram of the photocatalyst shows new reflections attributable to the metallic silver phase (JCPDS card #004-0783). The estimated loading of silver in this case was 3.6%wt, and an XRD analysis of a similar photocatalyst showed the same pattern [37]. The textural properties of the catalysts are reported in Table 2.

Table 2. Textural and optical properties of the photocatalysts employed.

Sample	Crystallite Size (nm)	Phase %	BG (eV)
P25	15 (A); 26 (R)	78 (A); 22 (R)	3.22
P25-500	18 (A); 25 (R)	90 (A); 10 (R)	3.12
Ag/P25-L	19 (A); 28 (R)	92 (A); 8 (R)	3.60

3.4.2. DRS UV–Vis

The band gaps of the photocatalysts were obtained from their absorption spectra, illustrated in Figure 5, using the Kubelka–Munk method and fitted with the Tauc equation. The samples all had indirect band gaps; thus, $r = \frac{1}{2}$ was used.

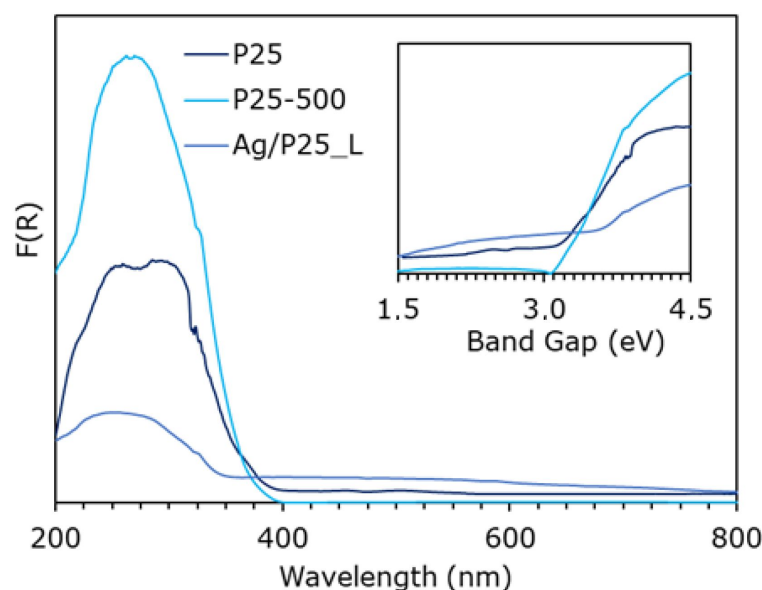


Figure 5. DR-UV spectra and band gap of immobilized titania, as such and decorated with Ag nanoparticles.

The absorption spectra obtained from the immobilized and impregnated P25 (with a 0.07 M solution of silver nitrate) show very interesting results. The latter's bandgap is much broader compared to that of P25 (3.6 eV, $1 \text{ eV} = 1.60218 \times 10^{-19} \text{ J}$), which is usually associated with a very high loading of silver NPs. This hypothesis is also confirmed by the XRD spectra, which shows reflections of Ag^0 , and by the broad adsorption band in the visible region due to localized surface plasmonic resonance (LSPR). The LSPR band is usually located around 460 nm, whereas here it is broader, since it is likely that Ag nanocluster are formed extensively on titania NPs [38,39]. The effect of co-catalyst addition is not always predictable on a band gap. The appearance of LSPR is almost always reported after Ag addition, while a red-shift of a blue-shift have been reported [40,41]. In particular, a blue-shift (also observed in our case) has been correlated with an increase in silver content due to the quantum confinement effect [41]. In addition, the thermally treated P25 retained its characteristic band gap (Figure 5). The optical properties of the catalysts are reported in Table 2.

3.4.3. SEM-EDX

SEM-EDX analysis has been performed on the commercial P25 powder and on both the deposited and impregnated P25. All the samples comprised a uniform array of titania nanoparticles at ca. 20 nm in size. The composition was checked via EDX, but as a result of the low metal loading, it was necessary to set the acquisition time to 12 min.

Figure S2a–c (see Supporting Information File) illustrate the growth of titania NPs that were thermally treated after deposition over glass and after the second impregnation cycle, which aimed to metallize the surface with silver. In addition, Ag loading was checked qualitatively via EDX, which confirmed the presence of the metal (2.2% wt) along with traces of Si that are probably due to glass debris. Results from the EDX analysis are reported in Figure S2f. Impregnation over a relatively high surface oxide as P25 usually results in good metal dispersion. An example of a uniform Ag dispersion, obtained for a Ag-P25 impregnated sample, is reported in Figure S3.

3.5. Net Irradiance Measurements and Evaluation

One of the problems of using dip-coated glass slides in this setup is that both faces of the glass are covered with titania (supposedly equally dispersed). Therefore, the face in front of the bulb receives most of the light, while the rear one is irradiated with the radiation either reflected by the wall of the photoreactor (not determined in our layout) or

that passes through the glass. To check whether all the immobilized catalyst contributes to the photocatalyzed reaction, an apparatus was built to evaluate the portion of the light absorbed by P25 on the rear face of the glass. The setup comprised a box containing a UV light source (i.e., a UV-LED lamp, 48 W, 365 nm, Suntech Ltd., Salisbury, UK) connected to a cylinder pipe through a hole, while on the other end of the pipe, the probe of a photoradiometer was placed (Figure 6). A 26 mm cut in the middle of the pipe allowed for the insertion of glass slides into its housing, in a way that left no gap and forced the light from the lamp to pass through the coated glasses. First, the background irradiance was collected and an uncoated glass slide was inserted into the apparatus. Then, we analyzed a batch of 15 glasses coated in the same session (recipe #9) with this setup by placing them in the housing, first with one face exposed to the lamp and then with the other one. Five of these glasses were carefully cleaned on one side to estimate the impact of just one layer on the attenuation of the radiation. Table 3 reports the results as functions of the weight of the deposited layer, assuming that it was evenly distributed over the two faces. It was found that the glass itself absorbed ca. 11.6% of the incident radiation, while the one-layer tiles absorbed, on average, 76.8% of the light that passed through, with a minimum of 73.4% and a maximum of 79.5%, upon subtraction of the attenuation due to the glass itself. As expected, the absorption increased when both sides were coated, with an average loss of irradiance of 84.7% (min. 83.0%, max. 86.3%).

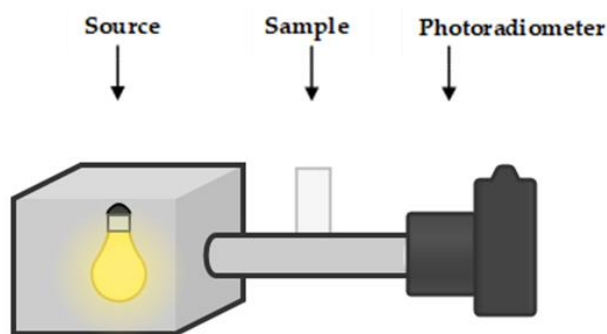


Figure 6. Setup used to measure the amount of light transmitted through the coated glasses.

Table 3. Attenuation measurements obtained after testing both single-side coated and full-coated glass slides.

Slide #	Side Coated	Loading (mg)	Mean Irradiance (mW/m ²)	Transmission (%)
none	/	/	825	100
uncoated	0	0	729	11.6
1.3	1	3.6	85.7	10.4
2.3	1	2.9	79.9	9.7
3.3	1	3.3	73.8	9.0
4.3	1	2.0	124	15.0
5.3	1	2.6	116	14.0
1.1	2	14.4	24.5	3.0
1.2	2	7.0	40.7	4.9
2.1	2	8.4	35.9	4.3
2.2	2	6.4	17.3	2.1
3.1	2	6.5	17.3	2.1
3.2	2	4.3	32.8	4.0
4.1	2	5.7	18.5	2.2
4.2	2	4.2	44.3	5.4
5.1	2	5.0	27.4	3.3
5.2	2	3.7	43.8	5.3

Therefore, on average, the rear face of the coated slide absorbed roughly 8% of the incident radiation. On one side, there was a waste of material that contributed only a fraction to the overall photocatalytic activity; on the other hand, this dip coating technique is very simple, and titania P25 is inexpensive. Thus, it is likely that this is still a favorable trade-off between the simplicity of the deposition technique and the inefficient usage of half of the photocatalyst. However, it should be underlined that the photoreactor is supplied with a reflective wall, and the rear face can contribute to light harvesting through direct irradiation.

3.6. Photoreforming over Supported Photocatalysts

Twelve slides coated with titanium dioxide (recipe #9) were mounted on the support with the final design, 3D printed in polypropylene reinforced with glass fiber. The overall mass of the deposited P25 was equal to 32 mg/L (comparable to the test carried out with powder P25, which used 31 mg/L). A total of 1.14 L of a glucose solution (5 g/L) was added to the photoreactor. The volume was reduced from the usual 1.20 L given that the extra volume added by the support and the slides was roughly 0.06 L. Tests were conducted for 5 h at 65 °C under 5 atm of nitrogen, first with just bare glass slides (blank test) and subsequently with P25 coated glass slides. In this case, we used unpromoted P25 since Ag did not prove to be effective as a photocatalyst for this application.

Figure 7 reports the results of this first test with the deposited catalyst. As expected, when bare glass was used, no photocatalytic activity was observed, and negligible glucose conversion (0.1%) occurred via photolysis. On the other hand, it was observed that the deposited P25 showed a productivity of hydrogen and carbon monoxide equal to 988 mmol/kg_{cat} h and 1455 mmol/kg_{cat} h, respectively. Commercial P25 powder in the same conditions showed a hydrogen productivity more than doubled (2500 mmol/kg_{cat} h) and a lower CO productivity (859 mmol/kg_{cat} h). The conversion of glucose also decreased from 6.5% (commercial P25 powder) to 4% (deposited sample) after 5 h of reaction.

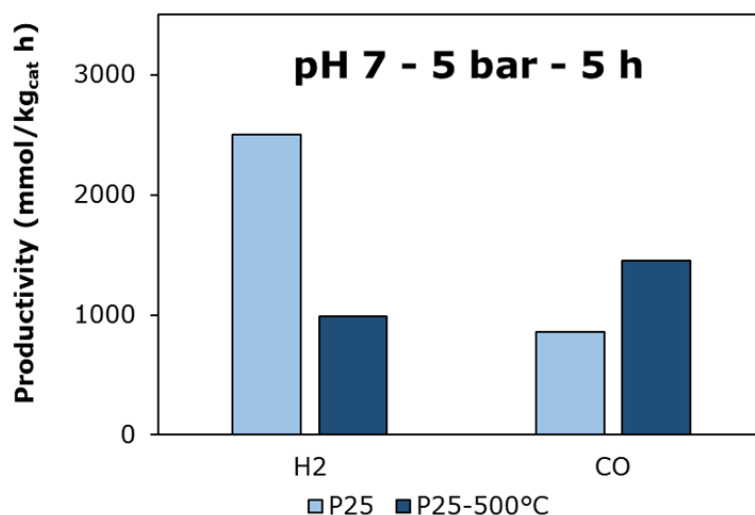


Figure 7. Glucose photoreforming carried out with P25 in the form of powder and the same catalyst immobilized. 65 °C, 1.14 L, 5 h, 5 bar N₂, 31 mg/L P25.

After the test, the glass tiles were dried and weighed again, and no weight loss was registered.

P25 retained its activity after the deposition process, although the productivity of H₂ decreased by roughly 60% while the amount of CO detected was higher. According to the XRD analysis, the deposited titania had a slightly higher percentage of anatase phase (90%) with respect to the untreated P25 (78%), while their crystallite sizes were comparable; therefore, this difference in the product distribution is explainable considering that, in powder form, the catalyst is fully accessible by reactants and light, while the deposited

material had a lower exposed and accessible surface. Indeed, as explained before, the dip coating technique causes the deposition of the photocatalyst on both the front and rear side of the glasses (assuming that the amount on the edges is negligible). In particular, the rear face of the coated slide absorbed roughly 8% of the incident radiation, leading to lower activity in half of the total deposited catalyst.

In the literature are some studies regarding the photoreforming of glycerol performed over a TiO₂-coated column, which show an H₂ productivity equal to 1580 mmol/kg_{cat} h [42]. Other authors reported that, when Pt was used as a co-catalyst, a slightly higher productivity of H₂ was obtained. In particular, Pt-loaded TiO₂ showed a productivity in the range of 1500–4300 mmol/kg_{cat} h [43–45]. The productivity of hydrogen reported with our deposited system is similar to the one observed in the photoreforming of glycerol over NiO/TiO₂ [46,47] and, although being lower than the deposited TiO₂ and Pt/TiO₂ systems previously described, remains comparable despite being an immobilized system. It should also be remarked that a higher activity in glycerol is expected with respect to glucose. The deposited P25 catalyst showed quite a high CO productivity. Furthermore, as previously stated, considering that the amount of the deposited catalyst effectively exposed to the UV radiation was roughly half of the total deposited mass, the results obtained are even more relevant.

A comparison of the deposited P25 productivity with the H₂ yield reported in the literature shows hydrogen productivities equal, respectively, to 360 mmol/kg_{cat} h and 720 mmol/kg_{cat} h. This was in experiments performed in the presence of methanol as a sacrificial agent (20%) with a lamp of 250 W over TiO₂ and FSP-TiO₂ [48,49].

3.7. Photoreduction of CO₂ over Deposited Photocatalysts

The consecutive/parallel reactions that took place are summarized in Scheme S1 (Supplementary Information).

A test was carried out on the immobilized titania modified via surface metallization with silver NPs (recipe #16; 0.01 M AgNO₃). The test was conducted at 80 °C with the help of a 3D support printed in polypropylene (PP) mixed with glass fibers, which was able to resist at the chosen temperature. Twelve glass tiles were used for the test with a cumulative loading corresponding to 50 mg/L (compared to the test with powder P25, which used 31 mg/L). A total of 1.67 g/L of sodium sulfite was used as HS in every case. The tests were performed under 18 bar of CO₂ for 24 h at pH 14. The glass tiles used for this test had an estimated Ag loading of 3.6% *w/w*. The results obtained from the tests are reported in Figure 8.

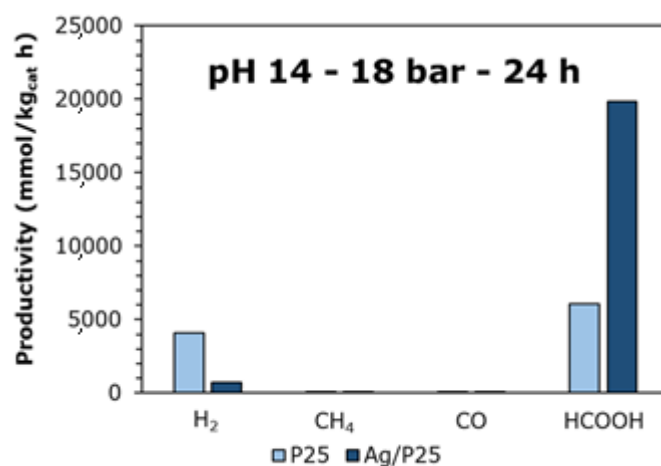


Figure 8. CO₂ photoreduction carried out with P25 in the form of powder and Ag/P25 immobilized. 80 °C, 1.14 L, 24 h, 18 bar CO₂, 1.67 g/L Na₂SO₃, 38 mg P25 or 50 mg Ag/P25.

The productivity of formic acid obtained with the Ag/P25 deposited catalyst was about three times the one obtained with the dispersed P25 powder, with values of ca. 20 mol/kg_{cat} h and 6 mol/kg_{cat} h, respectively. The deposited catalyst also showed a

productivity of hydrogen ca. that was one sixth of the one obtained in the test with the suspended P25 powder (ca. 0.7 mol/kg_{cat} h and 4 mol/kg_{cat} h, respectively). The production of H₂ is attributed to the consecutive photoreforming of the produced HCOOH after consumption of the inorganic hole scavenger (Scheme S1, Supplementary Information). Its lower productivity with the Ag-promoted sample testifies its lower activity in this reaction.

The productivities of methane and carbon monoxide were negligible during the test with the commercial P25 powder, while for the deposited Ag/P25, the productivity obtained was low but not nil. In particular, 15 mmol/kg_{cat} h and 37 mmol/kg_{cat} h were obtained for CH₄ and CO, respectively. The conversion of the hole scavenger due to the long reaction time was over 95% in both cases.

Additionally, the slides were collected after the test, washed with distilled water, and dried overnight at 105 °C, then weighed to verify any loss of catalyst during the test, which was found to be negligible.

Therefore, it is demonstrated that, to counteract the loss of activity due to surface coating, it is possible to tune the formulation of the catalyst, achieving an improvement of formic acid productivity with respect to bare P25 just by the addition of a simple metal co-catalyst.

The effects of silver deposition on titanium dioxide are indeed well known; this metal presents an LSPR band, thus enhancing visible light exploitation, though the catalyst was characterized by a wider band gap, and it improves the separation of the photogenerated charges by acting as an electron sink [50]. The lower hydrogen productivity of the Ag/P25-deposited catalyst suggests that the latter was less active in photoreforming the obtained organic products [51], thus preventing the consecutive consumption of formic acid.

Second, the deposited silver likely played a less active role in photoreforming the obtained species compared to the CO₂ photoreduction. In any case, the selectivity of the deposited catalyst towards liquid products should be further investigated.

Many authors have reported an increase in photocatalytic activity after functionalization [52–54]; however, being able to directly modify the immobilized titania through a simple dipping process and perform CO₂ photoreduction with such a system represents a great advancement for the technique. Indeed, examples of titanium dioxide are very frequent in the literature, but few cases of the immobilization of modified nanocatalysts or surface modification have been reported, and they may not be as scalable or flexible as the synthesis discussed here [55–57]. In addition, the recipes proposed here allow for the identification of an anchorage that lasts even in a demanding environment, such as high temperatures, wide pH variation, or a stirred liquid phase.

Multiple reviews can be found in the literature reporting relatively high productivity and selectivity, often using complex and expensive photocatalysts [5,58]. For example, some authors have reported a very high HCOOH productivity equal to 1100 mmol/kg_{cat} h using a mononuclear Ru complex deposited over C₃N₄ in the presence of *N,N*-dimethylacetamide and triethanolamine that acted as electron donor [59]. This HCOOH productivity, with the same hole scavenger conditions, can be further increased by using a binuclear Ru complex/Ag-loaded C₃N₄, which allows for the achievement of a productivity equal to 2115 mmol/kg_{cat} h [60]. Despite these interesting results, the main problem with these and many other catalysts reported in the literature relate to their high costs, since they use precious and rare metals such as ruthenium. Furthermore, they show relatively low productivity, and they have only been tested at a lab scale and not on a semi-pilot scale. With the high-pressure setup showed in this and in previous work, after optimizing the immobilization of P25 over glass tiles, and after developing a glass support that was able to withstand the harsh conditions present inside the photoreactor, we were able to achieve an HCOOH productivity of 20 mol/kg_{cat} h, which is unprecedented for immobilized catalysts. The low cost of the P25 and AgNO₃ used for the deposition, together with the high HCOOH productivity obtained and the elimination of the catalyst separation problem, demonstrates the feasibility of continuous photoreduction in the liquid phase.

4. Conclusions

Through a simple dip coating technique, we demonstrated that it is possible to immobilize titanium dioxide nanoparticles, in particular TiO₂ P25, over commercial glass tiles. The optimization of the process parameters, including a washing pre-treatment of the support, a heating post-treatment, and the temperature and pH of the titania dispersion, allowed us to obtain coatings on simple commercial glass slides of up to several milligrams of titania per dipping cycle. This can be increased to 100 mg via the addition of an inexpensive organic emulsifier that stabilizes the dispersion of titania in water. The deposited layer was tough enough under optimized conditions to be used for photocatalytic applications in the liquid phase and at high temperatures without incurring the detachment of the photocatalyst from the glass. The deposition procedure was optimized as follows: Microscope glass tiles were washed in a piranha solution, then in a bicarbonate solution, and finally rinsed in HCl (as reported in Supplementary Information). Once dried, TiO₂ deposition was performed through a dip-coating technique using a 15% *w/w* suspension of P25 (with addition of Dysperbik[®] as stabilizer). Calcination at 500 °C for 2 h allowed for the collection of the final tiles.

A study on the average irradiance that hit the front and rear sides of the glass slides showed that only 8% of the incident radiation was absorbed by the rear face of the coated slide, which may be further improved by using reflective walls in the photoreactor. This is one of the advantages of using immobilized photocatalysts, since they are a precisely located target for irradiation from a light source and this irradiance can be experimentally determined. This avoids the complex modeling of light irradiation, which is instead needed to theoretically interpret the photoreactors operating in slurry mode.

The use of the prepared slides for the photoreforming of glucose and for the photoreduction of CO₂ demonstrated that the photocatalytic activity of titania was overall retained after immobilization, although productivity was lower for the coated tiles than for the suspended powder, as expected. The further modification of the coated catalyst via simple dipping impregnation with a metal co-catalyst was sufficient to enhance its activity. Overall, a formic acid productivity of up to 20 mol/kg_{cat} h via the photoreduction of CO₂ was achieved, which is an extremely remarkable value when compared with the pertinent literature.

We believe that photocatalytic applications should be scaled up for practical application either in photosynthetic reactions or in the photocatalytic degradation of pollutants. In every case, a continuous operation mode should be foreseen, which implies the need for catalyst immobilization. So, in principle, this methodology can easily be extended to any photocatalytic or photosynthetic reaction.

The main limits of this technique reside in the overall amount of the catalyst that can be used, with respect to the suspended powder, but it allows for a larger powder coating than other more complex methods, such as CVD or PVD. The possibility of using pre-synthesized catalysts is also an advantage, allowing for fine control of the catalyst's properties. Adhesion properties may arise and can be further optimized by increasing surface roughness.

Supplementary Materials: The following supporting information can be downloaded at: <https://www.mdpi.com/article/10.3390/en16134990/s1>, Figure S1: (a) EDX analysis of a glass washed with H₂O; (b) EDX analysis of a glass washed with piranha solution (PS); (c) EDX analysis of a glass washed with PS and H₂O; (d) EDX analysis of a glass washed with PS and NaHCO₃ solution; (e) EDX analysis of a glass washed with PS, NaHCO₃ and HCl solutions; (f) EDX analysis of a reference glass washed with isopropyl alcohol; Figure S2: SEM images of the following samples: (a) SEM images of TiO₂ P25; (b) SEM images of P25 coated on glass and thermally treated at 500° (P25-500); (c) SEM images of P25 coated on glass and metallized with silver (Ag/P25-L); (d) SEM images of P25 coated on glass and thermally treated at 500 °C (P25-500), magnification 8000x; (e) SEM images of P25 coated on glass and metallized with silver (Ag/P25-L), magnification 10,000x; (f) SEM-EDX of P25 coated on glass and metallized with silver (Ag/P25-L). Figure S3: An example of Ag distribution after impregnation of P25 by SEM-EDX mapping. Table S1: Photocatalyst loading over

glass tiles after different pretreatments. Dipping in 5% w/w P25 suspension in distilled water, room temperature. Post-treatment was performed in a furnace at 500 °C for 1 h; Table S2. Photocatalyst loading over glasses obtained after several cycles. Dipping in 5% w/w P25 suspension in distilled water, room temperature. Post-treatment was performed in a furnace at 500 °C for 1 h; Table S3. Photocatalyst loading over glasses obtained with different temperatures and pH. Dipping in 5% w/w P25 suspension in distilled water, two cycles. Post-treatment was performed in a furnace at 500 °C for 1 h; Table S4. Photocatalyst loading over glasses obtained with different cycles of dip coating in 5% w/w P25 suspension in distilled water at pH 3 (HCl). Post-treatment was performed in a furnace at 500 °C for 1 h; Scheme S1. Consecutive pathways for CO₂ photoreduction and photoreforming occurring at basic pH.

Author Contributions: Conceptualization, F.C. and I.R.; methodology, M.I.A.; software, M.I.A.; validation, F.C., M.I.A. and M.T.; formal analysis, G.R.; investigation, M.T.; resources, F.C.; data curation, F.C.; writing—original draft preparation, M.T.; writing—review and editing, I.R.; visualization, F.C.; supervision, G.R.; project administration, I.R.; funding acquisition, I.R. All authors have read and agreed to the published version of the manuscript.

Funding: This research was funded by Fondazione Cariplo (Italy) through the grant “2021-0855 SCORE—Solar energy for circular CO₂ photoconversion and chemicals regeneration”, in the frame of the 2021 call on the circular economy (I. Rossetti, G. Ramis and M.I. Alam). This research is also part of the project “One Health Action Hub: University Task Force for the resilience of territorial ecosystems”, supported by Università degli Studi di Milano—PSR 2021—GSA—Linea 6 (I. Rossetti). This study was carried out within the Agritech National Research Center and received funding from the European Union Next-GenerationEU (PIANO NAZIONALE DI RIPRESA E RESILIENZA (PNRR)—MISSIONE 4 COMPONENTE 2, INVESTIMENTO 1.4—D.D. 1032 17/06/2022, CN00000022). This manuscript reflects only the authors’ views and opinions, neither the European Union nor the European Commission can be considered responsible for them. I. Rossetti and M. Tommasi acknowledge specifically the participation and funding of Tasks 8.2.3, 8.3.2, and 8.4.1.

Acknowledgments: The valuable help of the graduating student Igor Fontana is gratefully acknowledged. Alessandro Di Michele (University of Perugia) is gratefully acknowledged for the SEM-EDX mapping reported in Figure S3.

Conflicts of Interest: The authors declare no conflict of interest.

References

1. Alam, M.I.; Cheula, R.; Moroni, G.; Nardi, L.; Maestri, M. Mechanistic and multiscale aspects of thermo-catalytic CO₂ conversion to C 1 products. *Catal. Sci. Technol.* **2021**, *11*, 6601–6629. [[CrossRef](#)] [[PubMed](#)]
2. Tullo, A. Why the future of oil is in chemicals, not fuels. *Chem. Eng. News* **2019**, *97*, 26–29.
3. Garba, M.D.; Usman, M.; Khan, S.; Shehzad, F.; Galadima, A.; Ehsan, M.F.; Ghanem, A.S.; Humayun, M. CO₂ towards fuels: A review of catalytic conversion of carbon dioxide to hydrocarbons. *J. Environ. Chem. Eng.* **2021**, *9*, 104756. [[CrossRef](#)]
4. Green, M.A.; Emery, K. Solar cell efficiency tables (version 3). *Prog. Photovolt. Res. Appl.* **1994**, *2*, 27–34. [[CrossRef](#)]
5. Li, K.; An, X.; Park, K.H.; Khraisheh, M.; Tang, J. A critical review of CO₂ photoconversion: Catalysts and reactors. *Catal. Today* **2014**, *224*, 3–12. [[CrossRef](#)]
6. Shehzad, N.; Tahir, M.; Johari, K.; Murugesan, T.; Hussain, M. A critical review on TiO₂ based photocatalytic CO₂ reduction system: Strategies to improve efficiency. *J. CO₂ Util.* **2018**, *26*, 98–122. [[CrossRef](#)]
7. Thompson, W.A.; Sanchez Fernandez, E.; Maroto-Valer, M.M. Review and Analysis of CO₂ Photoreduction Kinetics. *ACS Sustain. Chem. Eng.* **2020**, *8*, 4677–4692. [[CrossRef](#)]
8. Fujishima, A.; Rao, T.N.; Tryk, D.A. Titanium dioxide photocatalysis. *J. Photochem. Photobiol. C Photochem. Rev.* **2000**, *1*, 1–21. [[CrossRef](#)]
9. Colmenares, J.C.; Luque, R. Heterogeneous photocatalytic nanomaterials: Prospects and challenges in selective transformations of biomass-derived compounds. *Chem. Soc. Rev.* **2014**, *43*, 765–778. [[CrossRef](#)]
10. Bahadori, E.; Ramis, G.; Zanardo, D.; Menegazzo, F.; Signoretto, M.; Gazzoli, D.; Pietrogiacomi, D.; Di Michele, A.; Rossetti, I. Photoreforming of glucose over CuO/TiO₂. *Catalysts* **2020**, *10*, 477. [[CrossRef](#)]
11. Conte, F.; Casalini, G.; Prati, L.; Ramis, G.; Rossetti, I. Photoreforming of model carbohydrate mixtures from pulping industry wastewaters. *Int. J. Hydrogen Energy* **2022**, *47*, 41236–41248. [[CrossRef](#)]
12. Nwosu, U.; Wang, A.; Palma, B.; Zhao, H.; Khan, M.A.; Kibria, M.; Hu, J. Selective biomass photoreforming for valuable chemicals and fuels: A critical review. *Renew. Sustain. Energy Rev.* **2021**, *148*, 111266. [[CrossRef](#)]
13. Clarizia, L.; Spasiano, D.; Di Somma, I.; Marotta, R.; Andreozzi, R.; Dionysiou, D.D. Copper modified-TiO₂ catalysts for hydrogen generation through photoreforming of organics. A short review. *Int. J. Hydrogen Energy* **2014**, *39*, 16812–16831. [[CrossRef](#)]

14. Toe, C.Y.; Tsounis, C.; Zhang, J.; Masood, H.; Gunawan, D.; Scott, J.; Amal, R. Advancing photoreforming of organics: Highlights on photocatalyst and system designs for selective oxidation reactions. *Energy Environ. Sci.* **2021**, *14*, 1140–1175. [[CrossRef](#)]
15. Si, Z.; Zhang, X.; Liu, Y.; Zhou, H.; Chen, X.; Yang, X.; Chen, H.; Zhan, J. Revisiting the preparation of titanium dioxide: Aerosol-assisted production of photocatalyst with higher catalytic activity than P25. *J. Mater. Sci.* **2020**, *55*, 565–576. [[CrossRef](#)]
16. Bahadori, E.; Tripodi, A.; Villa, A.; Pirola, C.; Prati, L.; Ramis, G.; Rossetti, I. High pressure photoreduction of CO₂: Effect of catalyst formulation, hole scavenger addition and operating conditions. *Catalysts* **2018**, *8*, 430. [[CrossRef](#)]
17. Ohtani, B.; Prieto-Mahaney, O.O.; Li, D.; Abe, R. What is Degussa (Evonic) P25? Crystalline composition analysis, reconstruction from isolated pure particles and photocatalytic activity test. *J. Photochem. Photobiol. A Chem.* **2010**, *216*, 179–182. [[CrossRef](#)]
18. Zakria, H.S.; Othman, M.H.D.; Kamaludin, R.; Sheikh Abdul Kadir, S.H.; Kurniawan, T.A.; Jilani, A. Immobilization techniques of a photocatalyst into and onto a polymer membrane for photocatalytic activity. *RSC Adv.* **2021**, *11*, 6985–7014. [[CrossRef](#)]
19. Wood, D.; Shaw, S.; Cawte, T.; Shanen, E.; Van Heyst, B. An overview of photocatalyst immobilization methods for air pollution remediation. *Chem. Eng. J.* **2020**, *391*, 123490. [[CrossRef](#)]
20. Forghieri, G.; Ghedini, E.; Menegazzo, F.; Di Michele, A.; Signoretto, M. An investigation on the photo-catalytic oxidation of air pollutants via SiO₂-supported TiO₂. *Appl. Catal. A Gen.* **2022**, *644*, 118813. [[CrossRef](#)]
21. Makula, P.; Pacia, M.; Macyk, W. How To Correctly Determine the Band Gap Energy of Modified Semiconductor Photocatalysts Based on UV-Vis Spectra. *J. Phys. Chem. Lett.* **2018**, *9*, 6814–6817. [[CrossRef](#)] [[PubMed](#)]
22. Tauc, J.; Grigorovici, R.; Vancu, A. Optical Properties and Electronic Structure of Amorphous Germanium. *Phys. Status Solidi* **1966**, *15*, 627–637. [[CrossRef](#)]
23. Rossetti, I.; Villa, A.; Pirola, C.; Prati, L.; Ramis, G. A novel high-pressure photoreactor for CO₂ photoconversion to fuels. *RSC Adv.* **2014**, *4*, 28883–28885. [[CrossRef](#)]
24. Olivo, A.; Ghedini, E.; Signoretto, M.; Compagnoni, M.; Rossetti, I. Liquid vs. gas phase CO₂ photoreduction process: Which is the effect of the reaction medium? *Energies* **2017**, *10*, 1394. [[CrossRef](#)]
25. Bahadori, E.; Tripodi, A.; Villa, A.; Pirola, C.; Prati, L.; Ramis, G.; Dimitratos, N.; Wang, D.; Rossetti, I. High pressure CO₂ photoreduction using Au/TiO₂: Unravelling the effect of co-catalysts and of titania polymorphs. *Catal. Sci. Technol.* **2019**, *9*, 2253–2265. [[CrossRef](#)]
26. Galli, F.; Compagnoni, M.; Vitali, D.; Pirola, C.; Bianchi, C.L.; Villa, A.; Prati, L.; Rossetti, I. CO₂ photoreduction at high pressure to both gas and liquid products over titanium dioxide. *Appl. Catal. B Environ.* **2017**, *200*, 386–391. [[CrossRef](#)]
27. Rossetti, I.; Bahadori, E.; Tripodi, A.; Ramis, G. Modelling of Photoreactors for Water Treatment. *Chem. Eng. Trans.* **2019**, *74*, 289–294. [[CrossRef](#)]
28. Meille, V. Review on methods to deposit catalysts on structured surfaces. *Appl. Catal. A Gen.* **2006**, *315*, 1–17. [[CrossRef](#)]
29. Srinivasa Rao, A. Effect of pH on the suspension stability of alumina, titania and their mixtures. *Ceram. Int.* **1987**, *13*, 233–241. [[CrossRef](#)]
30. Bahadori, E.; Conte, F.; Tripodi, A.; Ramis, G.; Rossetti, I. Photocatalytic Selective Oxidation of Ammonia in a Semi-Batch Reactor: Unravelling the Effect of Reaction Conditions and Metal Co-Catalysts. *Catalysts* **2021**, *11*, 209. [[CrossRef](#)]
31. Jang, J.I.; Jeong, H.C. Shear induced TiO₂ nano structure using brush-coating for liquid crystal alignment. *Crystals* **2020**, *10*, 860. [[CrossRef](#)]
32. Marques, M.E.; Mansur, A.A.P.; Mansur, H.S. Chemical functionalization of surfaces for building three-dimensional engineered biosensors. *Appl. Surf. Sci.* **2013**, *275*, 347–360. [[CrossRef](#)]
33. Behrens, S.H.; Grier, D.G. The Charge of Glass and Silica Surfaces. *J. Chem. Phys.* **2001**, *115*, 6716–6721. [[CrossRef](#)]
34. Greenwood, P.; Gevert, B.S.; Otterstedt, J.; Niklasson, G.; Vargas, W. Novel nano-composite particles: Titania-coated silica cores. *Pigment Resin Technol.* **2010**, *39*, 135–140. [[CrossRef](#)]
35. Zhang, Q.; Gao, L.; Guo, J. Effects of calcination on the photocatalytic properties of nanosized TiO₂ powders prepared by TiCl₄ hydrolysis. *Appl. Catal. B Environ.* **2000**, *26*, 207–215. [[CrossRef](#)]
36. Chen, Y.F.; Lee, C.Y.; Yeng, M.Y.; Chiu, H.T. The effect of calcination temperature on the crystallinity of TiO₂ nanopowders. *J. Cryst. Growth* **2003**, *247*, 363–370. [[CrossRef](#)]
37. Leong, K.H.; Gan, B.L.; Ibrahim, S.; Saravanan, P. Synthesis of surface plasmon resonance (SPR) triggered Ag/TiO₂ photocatalyst for degradation of endocrine disturbing compounds. *Appl. Surf. Sci.* **2014**, *319*, 128–135. [[CrossRef](#)]
38. Liu, L.; Zhang, X.; Yang, L.; Ren, L.; Wang, D.; Ye, J. Metal nanoparticles induced photocatalysis. *Natl. Sci. Rev.* **2017**, *4*, 761–780. [[CrossRef](#)]
39. Petica, A.; Florea, A.; Gaidau, C.; Balan, D.; Anicai, L. Synthesis and characterization of silver-titania nanocomposites prepared by electrochemical method with enhanced photocatalytic characteristics, antifungal and antimicrobial activity. *J. Mater. Res. Technol.* **2019**, *8*, 41–53. [[CrossRef](#)]
40. Ahmed, F.; Kanoun, M.B.; Awada, C.; Jonin, C.; Brevet, P.-F. An Experimental and Theoretical Study on the Effect of Silver Nanoparticles Concentration on the Structural, Morphological, Optical, and Electronic Properties of TiO₂ Nanocrystals. *Crystals* **2021**, *11*, 1488. [[CrossRef](#)]
41. Chalana, S.R.; Ganesan, V.; Mahadevan Pillai, V.P. Surface plasmon resonance in nanostructured Ag incorporated ZnS films. *AIP Adv.* **2015**, *5*, 107207. [[CrossRef](#)]

42. Skillen, N.; Ralphs, K.; Craig, D.; McCalmont, S.; Muzio, A.F.V.; O'Rourke, C.; Manyar, H.; Robertson, P.K.J. Photocatalytic reforming of glycerol to H₂ in a thin film Pt-TiO₂ recirculating photoreactor. *J. Chem. Technol. Biotechnol.* **2020**, *95*, 2619–2627. [[CrossRef](#)]
43. Vaiano, V.; Lara, M.A.; Iervolino, G.; Matarangolo, M.; Navio, J.A.; Hidalgo, M.C. Photocatalytic H₂ production from glycerol aqueous solutions over fluorinated Pt-TiO₂ with high {001} facet exposure. *J. Photochem. Photobiol. A Chem.* **2018**, *365*, 52–59. [[CrossRef](#)]
44. Paquin, F.; Rivnay, J.; Salleo, A.; Stingelin, N.; Silva, C. Multi-phase semicrystalline microstructures drive exciton dissociation in neat plastic semiconductors. *J. Mater. Chem. C* **2015**, *3*, 10715–10722. [[CrossRef](#)]
45. Slamet; Ratnawati; Gunlazuardi, J.; Dewi, E.L. Enhanced photocatalytic activity of Pt deposited on titania nanotube arrays for the hydrogen production with glycerol as a sacrificial agent. *Int. J. Hydrogen Energy* **2017**, *42*, 24014–24025. [[CrossRef](#)]
46. Fujita, S.; Kawamori, H.; Honda, D.; Yoshida, H.; Arai, M. Photocatalytic hydrogen production from aqueous glycerol solution using NiO/TiO₂ catalysts: Effects of preparation and reaction conditions. *Appl. Catal. B Environ.* **2016**, *181*, 818–824. [[CrossRef](#)]
47. Liu, R.; Yoshida, H.; Fujita, S.; Arai, M. Photocatalytic hydrogen production from glycerol and water with NiO_x/TiO₂ catalysts. *Appl. Catal. B Environ.* **2014**, *144*, 41–45. [[CrossRef](#)]
48. Chiarello, G.L.; Aguirre, M.H.; Selli, E. Hydrogen production by photocatalytic steam reforming of methanol on noble metal-modified TiO₂. *J. Catal.* **2010**, *273*, 182–190. [[CrossRef](#)]
49. Ahmad, H.; Kamarudin, S.K.; Minggu, L.J.; Kassim, M. Hydrogen from photo-catalytic water splitting process: A review. *Renew. Sustain. Energy Rev.* **2015**, *43*, 599–610. [[CrossRef](#)]
50. Zielińska-Jurek, A. Progress, challenge, and perspective of bimetallic TiO₂-based photocatalysts. *J. Nanomater.* **2014**, *2014*, 3. [[CrossRef](#)]
51. Ramis, G.; Bahadori, E.; Rossetti, I. Design of efficient photocatalytic processes for the production of hydrogen from biomass derived substrates. *Int. J. Hydrog. Energy* **2021**, *46*, 12105–12116. [[CrossRef](#)]
52. Yu, B.; Zhou, Y.; Li, P.; Tu, W.; Li, P.; Tang, L.; Ye, J.; Zou, Z. Photocatalytic reduction of CO₂ over Ag/TiO₂ nanocomposites prepared with a simple and rapid silver mirror method. *Nanoscale* **2016**, *8*, 11870–11874. [[CrossRef](#)] [[PubMed](#)]
53. Liu, E.; Hu, Y.; Li, H.; Tang, C.; Hu, X.; Fan, J.; Chen, Y.; Bian, J. Photoconversion of CO₂ to methanol over plasmonic Ag/TiO₂ nano-wire films enhanced by overlapped visible-light-harvesting nanostructures. *Ceram. Int.* **2015**, *41*, 1049–1057. [[CrossRef](#)]
54. Kočí, K.; Matějů, K.; Obalová, L.; Krejčíková, S.; Lacný, Z.; Plachá, D.; Čapek, L.; Hospodková, A.; Šolcová, O. Effect of silver doping on the TiO₂ for photocatalytic reduction of CO₂. *Appl. Catal. B Environ.* **2010**, *96*, 239–244. [[CrossRef](#)]
55. Lopes, F.C.S.; Maria da Graça, C.; Bargiela, P.; Ferreira, H.S.; Pires, C.A.D.M. Ag/TiO₂ photocatalyst immobilized onto modified natural fibers for photodegradation of anthracene. *Chem. Eng. Sci.* **2020**, *227*, 115939. [[CrossRef](#)]
56. van Grieken, R.; Marugán, J.; Sordo, C.; Martínez, P.; Pablos, C. Photocatalytic inactivation of bacteria in water using suspended and immobilized silver-TiO₂. *Appl. Catal. B Environ.* **2009**, *93*, 112–118. [[CrossRef](#)]
57. Lu, N.; Wang, Y.; Ning, S.; Zhao, W.; Qian, M.; Ma, Y.; Wang, J.; Fan, L.; Guan, J.; Yuan, X. Design of plasmonic Ag-TiO₂/H₃PW₁₂O₄₀ composite film with enhanced sunlight photocatalytic activity towards o-chlorophenol degradation. *Sci. Rep.* **2017**, *7*, 17298. [[CrossRef](#)]
58. Tan, J.Z.Y.; Maroto-Valer, M.M. A review of nanostructured non-titania photocatalysts and hole scavenging agents for CO₂ photoreduction processes. *J. Mater. Chem. A* **2019**, *7*, 9368–9385. [[CrossRef](#)]
59. Kuriki, R.; Sekizawa, K.; Ishitani, O.; Maeda, K. Visible-light-driven CO₂ reduction with carbon nitride: Enhancing the activity of ruthenium catalysts. *Angew. Chem.—Int. Ed.* **2015**, *54*, 2406–2409. [[CrossRef](#)]
60. Kuriki, R.; Matsunaga, H.; Nakashima, T.; Wada, K.; Yamakata, A.; Ishitani, O.; Maeda, K. Nature-Inspired, Highly Durable CO₂ Reduction System Consisting of a Binuclear Ruthenium(II) Complex and an Organic Semiconductor Using Visible Light. *J. Am. Chem. Soc.* **2016**, *138*, 5159–5170. [[CrossRef](#)]

Disclaimer/Publisher's Note: The statements, opinions and data contained in all publications are solely those of the individual author(s) and contributor(s) and not of MDPI and/or the editor(s). MDPI and/or the editor(s) disclaim responsibility for any injury to people or property resulting from any ideas, methods, instructions or products referred to in the content.